## The effect of damage on reloading

The hybrid gel suffers internal damage after the first loading. To study the effect of the damage, we loaded a sample of the hybrid gel up to a certain stretch λ_{max}, unloaded the gel to zero force, and followed with a second loading. The fracture energy measured on the second loading was reduced from that measured on the first loading (Supplementary Fig. 1). The amount of reduction increased with the maximum stretch of the first loading. The gel regained some fracture energy if the second loading was applied 1 day later. The fracture energy was determined by using a procedure described at the end of the supplementary information.
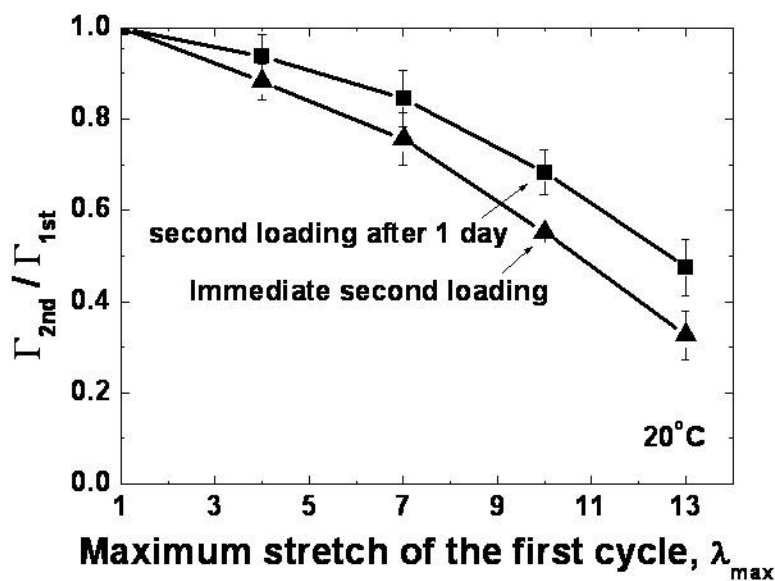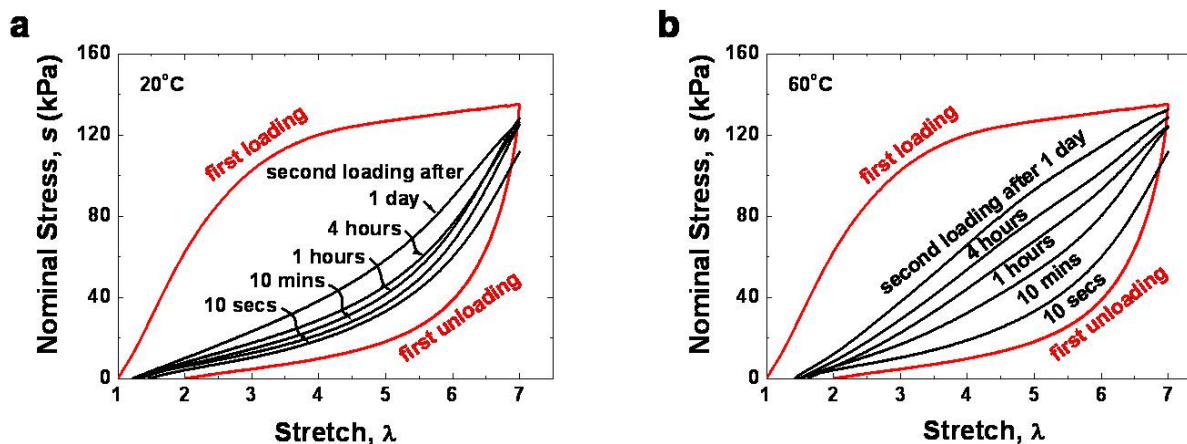
Supplementary Figure 1 | Damage after the first cycle. The hybrid gel was first loaded to a certain maximum stretch λ_{max}, and was then unloaded to zero force, followed by a second loading. The fracture energy determined on the second loading Γ_{2nd} was reduced from that determined on the first loading Γ_{1st}. The alginate-to-acrylamide ratio was 1:6. The covalent crosslinker, MBAA, was fixed at 0.0006 the weight of acrylamide. The ionic crosslinker, $CaSO_4$, was fixed at 0.1328 the weight of alginate. (Error bars, S.D.; n=3).

Recovery after the first loading: the effect of storage time and temperature

The recovery after the first loading takes time, and can be made faster by storing the gel in a hot bath. A sample of the hybrid gel was first loaded in tension to a stretch of 7, and was unloaded to zero force. The sample was then sealed in a polyethylene bag and submerged in mineral oil to prevent water from evaporation, and stored in a bath of a fixed temperature for a

certain period of time. Afterwards the sample was taken out of storage and its stress-stretch curve was measured again at room temperature. Supplementary Fig. 2 shows the stress-stretch curve on the first loading and unloading, as well as the stress-stretch curves on the second loading after the sample was stored at certain temperatures for certain periods of time. In the second loading, the gel was weaker than the first loading. The extent of recovery increased with the temperature and time of storage.

Supplementary Figure 2 | Recovery after the first loading. Each hybrid gel sample was first loaded to a stretch of $\lambda = 7$, and then unloaded. The samples were then stored at a certain temperature for a period time, followed by a second loading at room temperature. Stress-stretch curves are shown for samples stored at: **a**, 20 ℃; **b,** 60 ℃. The alginate-to-acrylamide ratio was 1:6. The covalent crosslinker, MBAA, was fixed at 0.0006 the weight of acrylamide. The ionic crosslinker, $CaSO_4$, was fixed at 0.1328 the weight of alginate.

Effect of the ionic crosslink density of alginate

To study the effect of the ionic crosslinks between alginate chains, we prepared hybrid gels with various concentrations of $CaSO_4$ (Supplementary Fig. 3). For the unnotched samples, the stress needed to deform the gel increased with the concentration of $CaSO_4$. The small-strain elastic modulus increased with the concentration of $CaSO_4$. For the notched samples, however, the critical stretch for the notch to turn into a running crack decreased as the concentration of $CaSO_4$ increased. The highest fracture energy was obtained for an intermediate concentration of $CaSO_4$. These trends are understood as follows. In the absence of Ca^{++}, alginate chains are not crosslinked, and bear no load, so that the hybrid gel exhibits a stress-stretch curve indistinguishable from that of the polyacrylamide gel, with large stretchability but low fracture energy. At a high concentration of Ca^{++}, alginate chains are densely crosslinked. Only a small zone around the root of the notch is stressed enough to break the alginate chains, so the fracture energy is low.
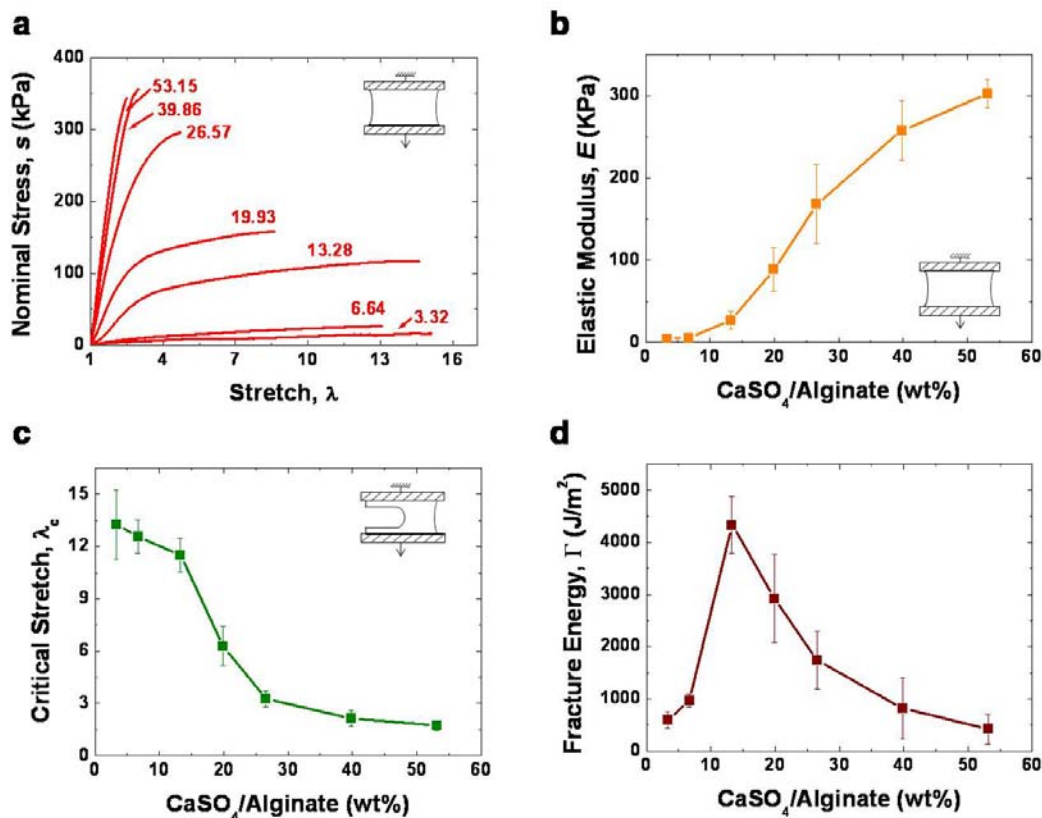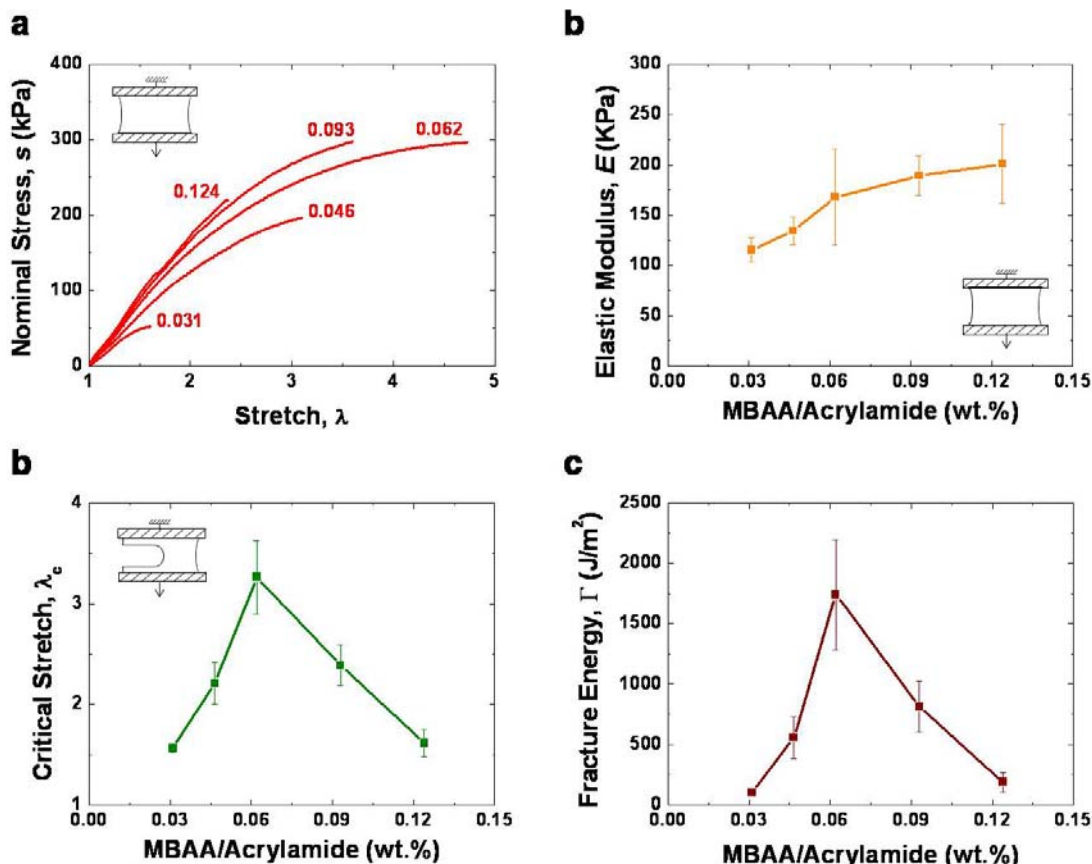
Supplementary Figure 3 | The amount of ionic crosslinker, CaSO₄, greatly affects the behavior of the hybrid gel. **a**, Stress-strain curves were measured using unnotched samples of gels of various values of CaSO$_4$/Alginate (wt%). **b**, Elastic moduli were determined by the initial slopes of the stress-strain curves. **c**, The critical stretches were measured using notched samples of gels. **d**, Fracture energy varies with the density of the ionic crosslinker. The weight ratio of alginate to acrylamide was fixed at 1:10, and the water content was fixed at 86 wt %. The covalent crosslinker, MBAA, was fixed at 0.0006 the weight of acrylamide. (Error bars, S.D.; n=3).

Effect of the covalent crosslink density of polyacrylamide

To study the effect of the covalent crosslinks of polyacrylamide, we prepared hybrid gels with various concentrations of the crosslinker MBAA. Properties of these gels are shown in Supplementary Fig. 4. As the concentration of MBAA increased, the crosslink density of the polyacrylamide network increased. However, the stiffness of the hybrid gel increased only slightly. The concentration of MBAA did greatly affect the critical stretches of the notched samples. The highest fracture energy was obtained for an intermediate concentration of MBAA. This trend is understood as follows. When the covalent crosslink density is too high, each individual polyacrylamide chain between two crosslinks is short. When the chain breaks, the energy stored in the entire chain is dissipated. Consequently, shorter chains will lead to low fracture energy. In the other extreme, when the covalent crosslink density is too low, the polyacrylamide network becomes too compliant, incapable to stabilize the deformation of the gel.

Consequently, deformation in a notched gel is localized: only a small part of the alginate network will unzip and dissipate energy.

Supplementary Figure 4 | The amount of covalent crosslinker, MBAA, greatly affects the behavior of the hybrid gel. **a**, Stress-strain curves were measured using unnotched samples of gels of various values of MBAA/Acrylamide (wt%). **b**, Elastic moduli were determined from the initial slopes of the stress-strain curves. **c**, The critical stretches were measured using notched samples of gels. **d**, Fracture energy varies with the concentration of the covalent crosslinker. The weight ratio of alginate to acrylamide was fixed at 1:10, and the water content was fixed at 86 wt %. The ionic crosslinker, $CaSO_4$, was fixed at 0.1328 the weight of alginate. (Error bars, S.D.; n=3).

The effect of the crosslinker density on alginate hydrogels

Mechanical properties were measured for alginate hydrogels of various $CaSO_4$ concentrations (Supplementary Fig. 5). For the unnotched samples, the stress needed to deform the gel increased with the concentration of $CaSO_4$. For the notched samples, however, the critical stretch for the notch to turn into a running crack decreased as the concentration of $CaSO_4$ increased. The highest fracture energy was obtained for an intermediate concentration of $CaSO_4$.
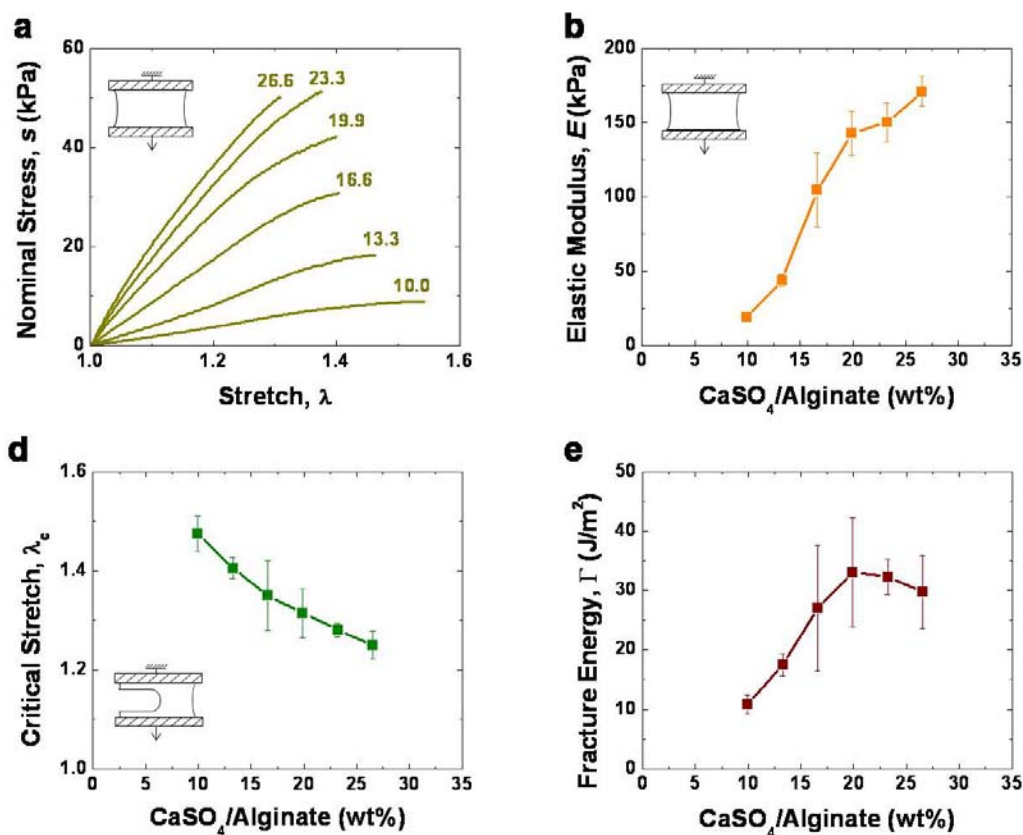
Supplementary Figure 5 | The mechanical behavior of alginate hydrogels with various crosslinker densities. **a**, Stress-strain curves were measured using unnotched samples of gels of various values of $CaSO_4$/Alginate (wt%). **b**, Elastic moduli were calculated from stress-strain curves. **c**, The critical stretches were measured using notched samples of gels. **d**, Fracture energy varies with the density of the ionic crosslinker. (Error bars, S.D.; n=3). Water content was fixed at 97 wt.%. (The solubility of alginate in water is less than 4 wt.%.)

The effect of crosslinker density on polyacrylamide hydrogels

Mechanical properties were measured for the polyacrylamide hydrogels of various MBAA concentrations (Supplementary Fig. 6). As the concentration of MBAA increased, the stiffness of the hybrid gel increased. However, the critical stretch of the notched samples decreased dramatically, the highest fracture energy was obtained for the minimum concentration of MBAA. Polyacrylamide single network gels with smaller than 0.015 wt.% MBAA concentration were only a viscous liquid after crosslinking.
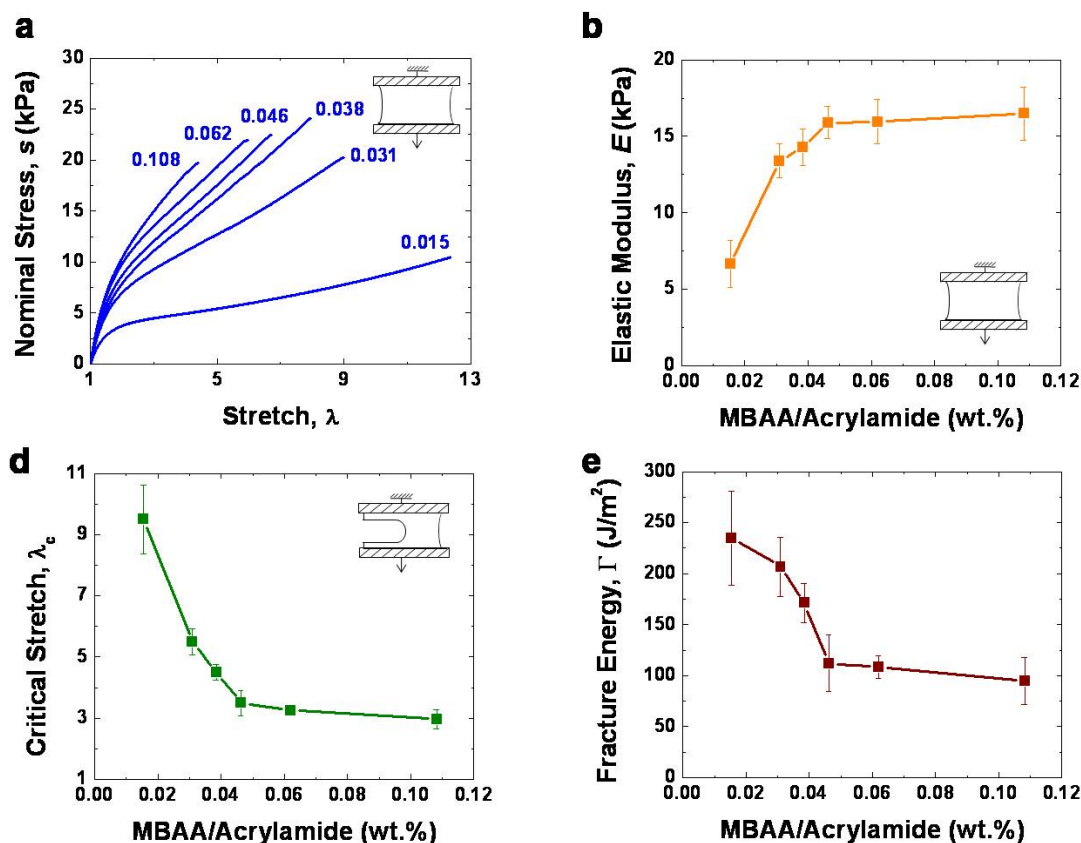
Supplementary Figure 6 | The mechanical behavior of polyacrylamide hydrogels with various crosslinker densities. **a**, Stress-strain curves were measured using unnotched samples of gels of various values of MBAA/Acrylamide (wt%). **b**, Elastic moduli were calculated from stress-strain curves. **c**, The critical stretches were measured using notched samples of gels. **d**, Fracture energy varies with the concentration of the covalent crosslinker. Water content was fixed at 86.4 wt.%. (Error bars, S.D.; n=3).

Viscoelastic responses determined by dynamic mechanical analysis (DMA)

The viscoelastic responses of alginate, polyacrylamide, and alginate-polyacrylamide hybrid gels were determined by using DMA Q800 (TA Instruments). Compression frequency-sweep tests at 0.1% strain were carried out over the frequency range 0.01-30 Hz. Alginate gels with 97%, polyacrylamide gels with 86.4 wt.%, and alginate-polyacrylamide hybrid gels with 86.4 wt.% water concentration were used for this test. The polymer ratio of alginate-polyacrylamide hybrid gel is 1:6 of alginate to acrylamide. The covalent crosslinker, MBAA, was fixed at 0.0006 the weight of acrylamide for polyacrylamide gel and hybrid gel. The ionic crosslinker, $CaSO_4$, was fixed at 0.1328 the weight of alginate for alginate gel and hybrid gel.

The storage modulus E' and the loss modulus E'' for alginate, polyacrylamide, and hybrid gels were determined as the frequency changes (Supplementary Fig. 7). The ratio of E''/E' indicates the viscosity of the material. As expected, due to the unzipping behavior of the alginate network, alginate and hybrid gels show more viscous behavior than the polyacrylamide gels. Furthermore, alginate gels and alginate-polyacrylamide hybrid gels clearly show the

increase of E'' at high frequency. The high frequency rise in E'' reflects fast relaxation processes and is typical viscous behavior of gels formed by temporary (breakable) junction zones [31].
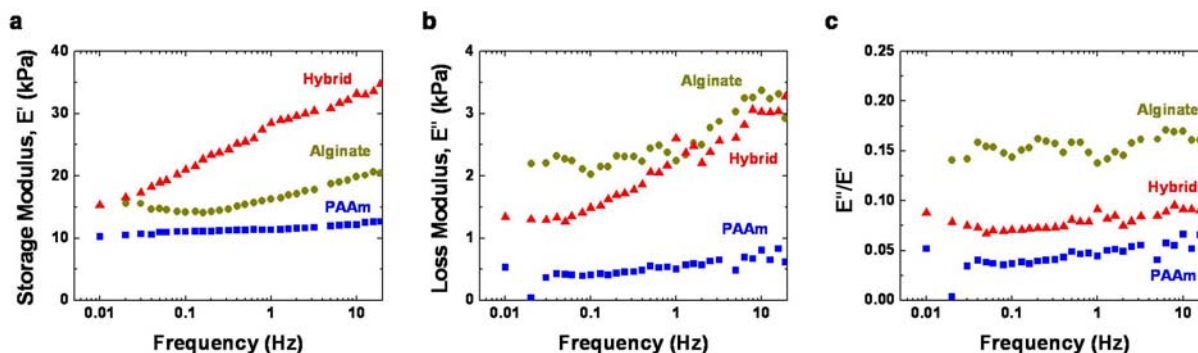

Supplementary Figure 7 | Viscoelasticity of alginate, polyacrylamide, and hybrid gels. **a**, Storage modulus E'. **b**, Loss modulus E''. **c**, The ratio between E'' and E'.

Homogeneity of hybrid gels

The homogeneity of alginate-polyacrylamide hybrid gels was investigated in two ways. First, the homogeneity of alginate networks in hybrid gels were tested using fluorescence images of hybrid gels which were fabricated from fluorescent alginate. Second, since the amount of calcium ion was strongly related to the elastic modulus of hybrid gels, the homogeneity of the calcium ions was explored by performing elastic modulus mapping of the surface of the hybrid gel. Alginate-polyacrylamide hybrid gels with 1:6 polymer ratio, 0.0006 MBAA concentration, 0.1328 $CaSO_4$ concentration, and 86.4 wt.% water concentration were used for these tests. Fluorescent alginate was prepared by coupling aminofluorescein (Sigma) to alginate polymers following same procedure as our previous work [2]. Fluorescence images were taken using a 1.40 NA 63X PlanApo oil immersion objective on a laser scanning confocal microscope (Zeiss LSM710). As demonstrated by a representative image (Supplementary Fig. 8a), the fluorescent alginate (shown in green) is fully interpenetrating and uniformly distributed within the hybrid gel.

The elastic modulus mapping is performed using atomic force microscope (Asylum-1 MFP-3D AFM System) with silicon nitride cantilever (Bruker AFM probes) with pyramid tipped probes. The stiffness of cantilevers is calibrated from thermal fluctuations (~35 pN/nm). To reduce the effect of the surface tension of the hydrogel, force measurements were performed in water with a 1000 nm/s sample surface movement. A 500 μm $\times$ 500 μm surface area of the hybrid gel is scanned and 6 $\times$ 6 points are examined with a 100 μm distance between each point. The elastic moduli were calculated from the relationship between indentation depth δ and punch load F using the Hertzian model for a pyramid punch [3]. The resulting elastic moduli of hybrid gels and their distribution are plotted in Supplementary Fig. 8c and d, respectively. An average 10.0 kPa elastic modulus was obtained with 2.7 kPa standard deviation.
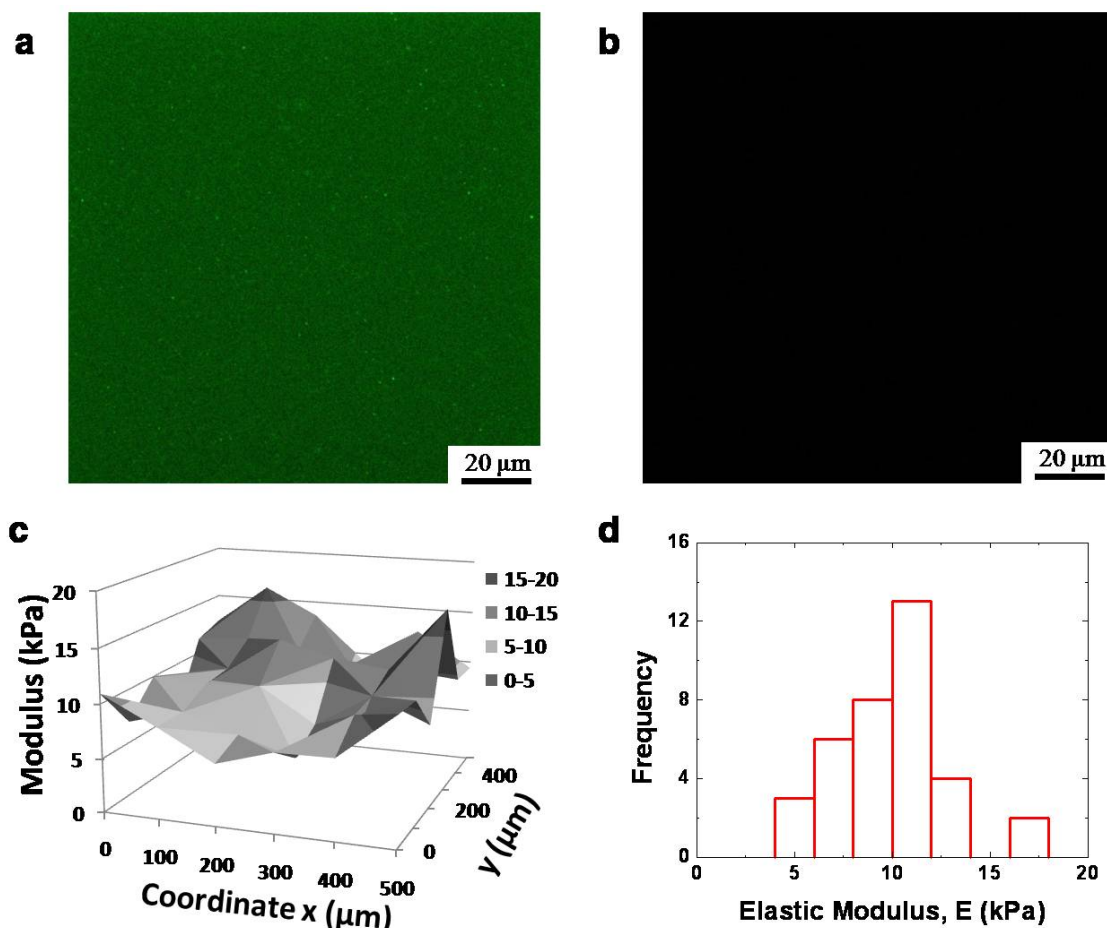
Supplementary Figure 8 | Homogeneity of hybrid gel. Fluorescence microscopy of hybrid gel mixed with fluorescent alginate (**a**) and without fluorescent alginate (**b**). **c**, Elastic modulus map of hybrid gel. **d**, Statistical plot of elastic modulus.

Crosslinks between alginate and polyacrylamide.

As mentioned before, the stress-stretch curves of the hybrid gels clearly indicate that both alginate and polyacrylamide bear loads. The mechanism of load-transfer between the two types of polymers is unclear. To investigate possible crosslinks between the two types of polymers, we analyzed the Fourier Transform Infrared (FTIR) spectra of the alginate gel, polyacrylamide gel, and hybrid gel. Samples of the same thickness ($\approx$100 μm) were prepared for the alginate gel, the polyacrylamide gel, and the alginate-acrylamide hybrid gel. They were frozen at -20 ℃ and dried in vacuum chamber for 2 days to eliminate water molecules from the samples. FTIR spectra were recorded between 4000 and 400 cm^{-1} on a Nicolet 360 FTIR E.S.P. spectrometer.

The FTIR spectra of the three gels are shown in Supplementary Fig. 9. The alginate gel showed a broad peak near 3400 cm^{-1} for O-H stretching, one sharp peak at 1620 cm^{-1} for asymmetric COO- stretching, two peaks at 1420 and 1320 cm^{-1} for C-H deformation with secondary alcohols, and three peaks at 1120, 1090, and 1030 cm^{-1} for asymmetric C-O-C

stretching, C-O stretching in CH-OH structure, and symmetric C-O stretching in C-O-C structure, respectively. The polyacrylamide gel exhibited bands at 3360 cm^{-1} and 3200 cm^{-1}, corresponding to a stretching vibration of N-H, and at 1670 cm^{-1} for C=O stretching. The bands at 1620 cm^{-1} (N-H deformation for primary amine), 1450 cm^{-1} (CH$_2$ in-plane scissoring), 1420 cm^{-1} (C-N stretching for primary amide), 1350 cm^{-1} (C-H deformation), and 1120 cm^{-1} (NH$_2$ in-plane rocking) were also detected. The spectra of the hybrid gel were characterized by comparing the presence of the absorption bands with the pure components. In the spectra of the hybrid gel, a new peak at 1280 cm^{-1} for C-N stretching of secondary amide was created. Furthermore, the intensity of the absorption bands (1620, 1420 cm^{-1}) which are related with primary amide, and the intensity of NH$_2$ in-plane rocking peak (1120 cm^{-1}) were decreased. Moreover, the intensities of O-H stretching peak (3400 cm^{-1}), C-O stretching in CH-OH structure (1090 cm^{-1}), and symmetric C-O stretching in C-O-C structure (1030 cm^{-1}) were decreased. This result indicates new bonds formed between -NH$_2$ groups of polyacrylamide and carboxyl groups of alginate.
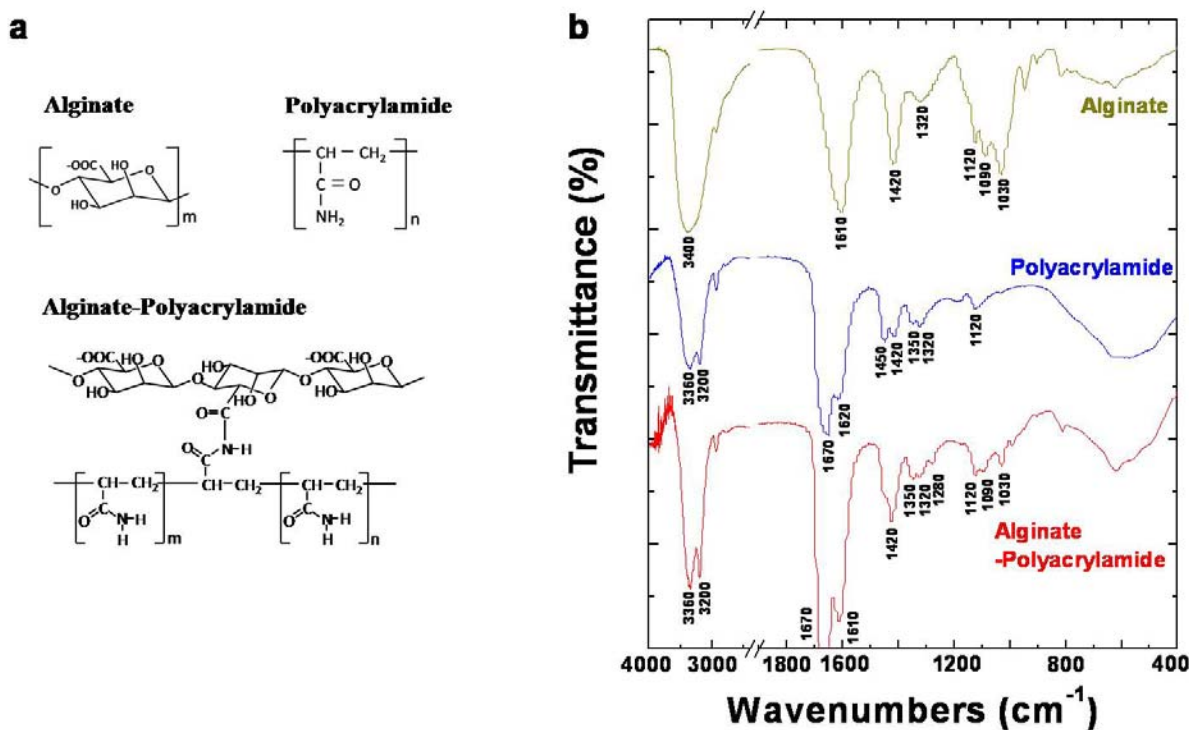

Supplementary Figure 9 | Crosslinks between alginate and polyacrylamide. **a**, Chemical structures of alginate and polyacrylamide, and suggested crosslinks between alginate and polyacrylamide. **b**, FTIR spectra alginate, polyacrylamide, and alginate-polyacrylamide hybrid.

Thermogravimetric analysis (TGA)

To confirm the two gel networks were covalently coupled, the thermal degradation of the alginate, polyacrylamide, and alginate-polyacrylamide hybrid gels were studied using TGA Q5000 (TA Instruments), under a nitrogen atmosphere at a heating rate of 10 ℃/min. Samples

were scanned from 40 to 750 ℃. Alginate-polyacrylamide hybrid gel with the polymer ratio 1:6 of alginate to acrylamide was used for this test. Gel samples were frozen at -80 ℃ and dried in vacuum for a week, then the gels were ground with a mortar. Samples ranging between 4 and 8 mg in weight were tested in platinum pans.

The integral results from the thermogravimetric analysis (TGA) are shown in Supplementary Fig. 10a, while the differential thermogravimetric data (DTG) are reported in Supplementary Fig. 10b, for alginate, polyacrylamide, and alginate-polyacrylamide hybrid gels. DTG data were deduced from TGA data by the derivative of the weight loss percent with respect to time. Each peak in DTG curves represents the temperature where the degradation rate is maximum for each degradation stage in the whole process. It is found that alginate has two pyrolysis stages, the first thermal degradation process occurred in the temperature range 225-300 ℃. The weight loss in first stage is attributed to the degradation of the carboxyl group, as CO_2 is released. The second stage occurred in the range 650-740 ℃, and is attributed to the depolymerization of polymer and formation of a carbonaceous residue, and finally yields $CaCO_3$ as char [34]. The thermal degradation of polyacrylamide occurs in three pyrolysis stages. In the temperature range 230-330 ℃, one ammonia molecule is liberated for every two amide groups, resulting in the formation of imide [35]. Subsequently, thermal degradation of imides and breaking of the polymer backbone occurs as the second and third stages, as suggested by Burrows et al. Alginate-Polyacrylamide hybrid gel clearly shows three pyrolysis stages instead of the five stages which would result from the sum of the individual materials. Moreover the locations of the second and third stages of hybrid gel are shifted from the locations of the single networks. Complete chemical analysis from the degradation of hybrid gels is difficult. However, by comparing the trend with previous graft interpenetrating polymers [36-39], the reduced number of pyrolysis stages and shifted peak locations of DTG qualitatively support the formation of new covalent bonds between alginate and polyacrylamide.
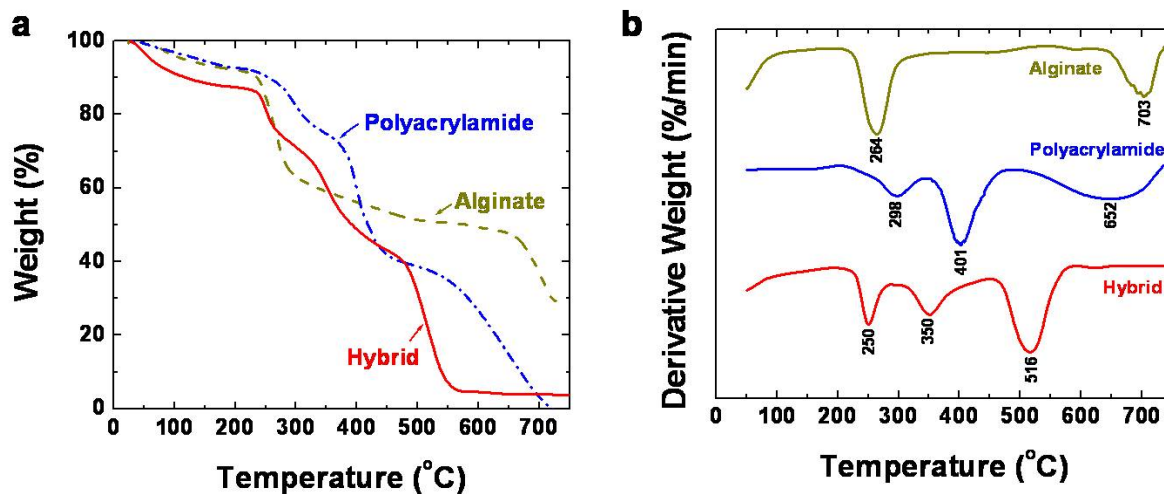
Supplementary Figure 10 | The thermal degradation of alginate, polyacrylamide, and alginate-polyacrylamide hybrid gels. **a**, Data of thermogravimetric analysis (TGA). **b**, Data of differential thermogravimetry (DTG).

Energy-dissipating mechanisms in three types of gels

When a notched gel is stretched, the deformation is inhomogeneous: the polymer chains directly ahead of the notch are stretched more than the chains elsewhere (Supplementary Fig. 11). For the notch in the polyacrylamide gel to turn into a running crack, only the chains directly ahead of the notch need to break. For the notch in the alginate gel to turn into a running crack, only the network directly ahead of the notch need to unzip. In either case, the gel is notch-sensitive because energy dissipates over a highly localized region: only a tiny fraction of the chains in the network—those crossing the crack plane—participate in energy dissipation. By contrast, in the hybrid gel, the number of chains that participate in energy dissipation is dramatically increased. For the notch in the hybrid gel to turn into a running crack, the chains directly ahead of the notch need to break. But before these chains break, the alginate network unzips over a large zone around the root of notch. This is likely the result of the efficient energy transfer between the two networks, due to their direct coupling, that results in alginate chains in a large zone being subjected to stress.

Polyacrylamide gel   **Alginate gel**   **Hybrid gel**

Plastic zone near the crack tip
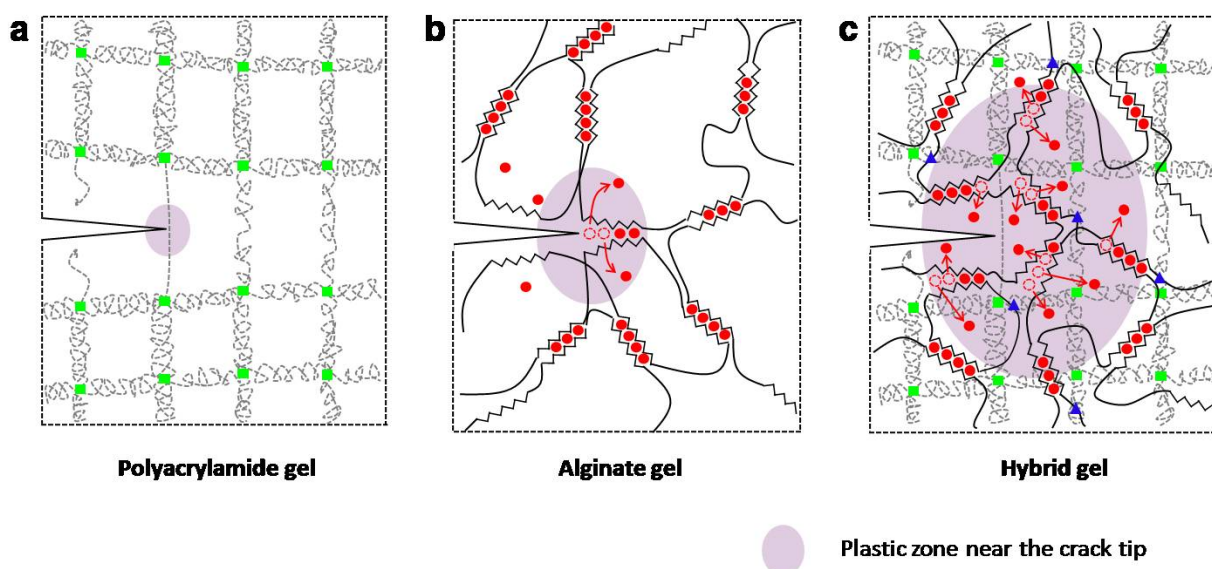
Supplementary Figure 11 | Synergy between alginate and polyacrylamide. **a,** In the polyacrylamide gel, for the notch to turn into a running crack, only the polyacrylamide chains crossing the crack plane need to break, and chains elsewhere remain intact. **b,** In the alginate gel, for the notch to turn into a running crack, only the ionic crosslinks for the chains crossing the crack need to break, and ionic crosslinks elsewhere remain intact. **c,** In the hybrid gel, the polyacrylamide chains bridge the crack and stabilize deformation in the background, the chemical interactions between the networks transfer the load over a large zone, and the ionic crosslinks between alginate chains break and provide inelastic deformation over this large zone around the root of the notch.
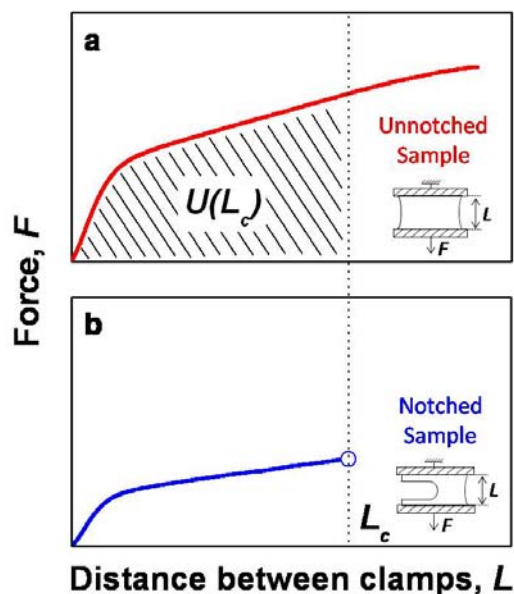
Determination of fracture energy

We determined the fracture energy of a gel using a method introduced by Rivlin and Thomas [40]. To adapt the method to measure the fracture energy of an extremely stretchable gel, we separately pulled two samples of the same gel (Supplementary Fig. 12). One sample was

unnotched, and the other sample was notched. In the initial state when the gel was undeformed, each sample was of width a_o = 75 mm and thickness b_o = 3 mm, and the distance between the two clamps was L_o = 5 mm. The unnotched sample was pulled to measure the force-length curve. (To determine the fracture energy, it was unnecessary to pull the unnotched sample all the way to rupture.) When the two clamps were pulled to a distance L, the area beneath the force-length curve gave the work done by the applied force, $U(L)$. The notched sample was prepared by using a razor blade to cut into the gel a 40 mm-long notch. (The precise length of the notch was unimportant for this test.) The notched sample was pulled, and pictures were taken at a rate of ~30 frames/sec to record the critical distance between the clamps, L_c, when the notch turned into a running crack. The fracture energy was calculated from

$$\Gamma = \frac{U(L_c)}{a_o b_o} .$$

We verified this method with two other methods described by Rivlin and Thomas [S10]: the tensile test with multiple samples containing notches of various lengths, and the double-peeling test. Although the notch turned into a running crack when the sample was pulled to a huge length, the fracture energy determined by all three methods matched well. Even though the entire sample underwent inelastic deformation, the method is still expected to yield a valid test for fracture energy. The situation is similar to testing very ductile metals under large-scale yielding conditions [41].

Supplementary Figure 12 | Experimental determination of fracture energy. Two samples of the same gel were tested in tension. One sample was unnotched, and the other sample was notched. **a**, The unnotched sample was used to measure the force-length curve. The area beneath the force-length curve gave the work done by the force to the unnotched sample, $U(L)$. **b**, The notched sample was used to measure the critical distance between the clamps, L_c, when the notch turned into a running crack.

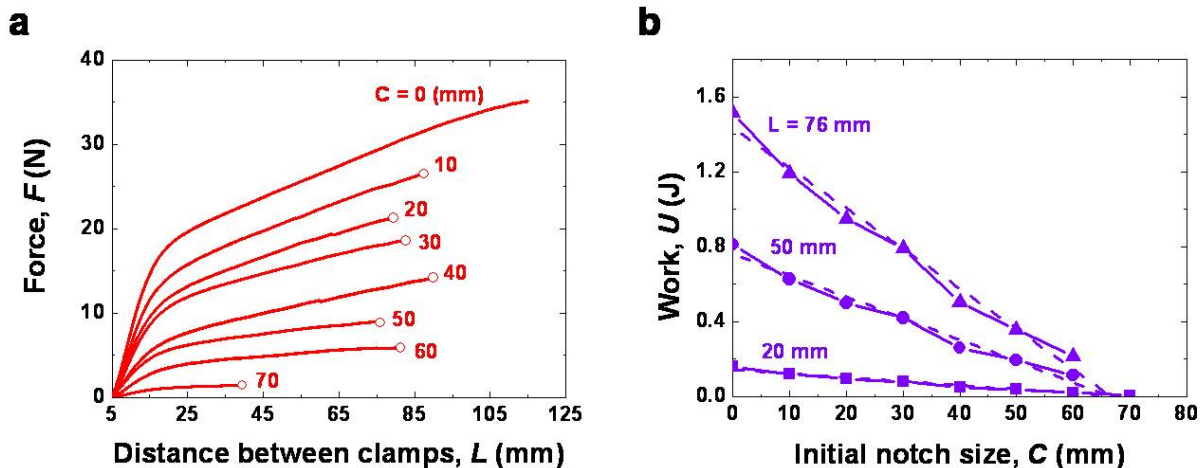## Tensile test with samples of various crack lengths

The pure-shear test was verified with two other tests: tensile test with samples of various crack lengths and double peeling test [S10]. Alginate-polyacrylamide hybrid gels with 1:8 polymer ratio, 0.0006 MBAA concentration, 0.1328 $CaSO_4$ concentration, and 86.4 wt.% water concentration were used for this verification.

First, tensile tests with various initial crack sizes were used to obtain fracture energy. Samples with dimensions $L_0 = 5mm$, $a_0 = 75mm$ and $b_0 = 3mm$ were prepared with various crack lengths, C. The configuration of the test is the same as shown in Supplementary Fig. 12. Force-extension curves were obtained until the onset of crack propagation occurred. L is the change in distance between the clamps. The total energy U stored in the test piece at deformation L is obtained by measuring the area under the force-extension curve and U is plotted with the crack lengths, C as shown in Supplementary Fig. 13b. A suitable L value is selected in a way that it corresponds to L of at least one fractured sample. $\left(\frac{\partial U}{\partial C}\right)_L$ is calculated from the slope of the total energy vs crack length curve. Thus the fracture energy is given by,

$$\Gamma = \frac{1}{b_0}\left(\frac{\partial U}{\partial C}\right)_L$$

Using this method with L = 76 mm, the fracture energy obtained is $7158 \pm 400 \frac{J}{m^2}$ which is comparable with the value 7350 J/m² which is obtained from the pure-shear test.
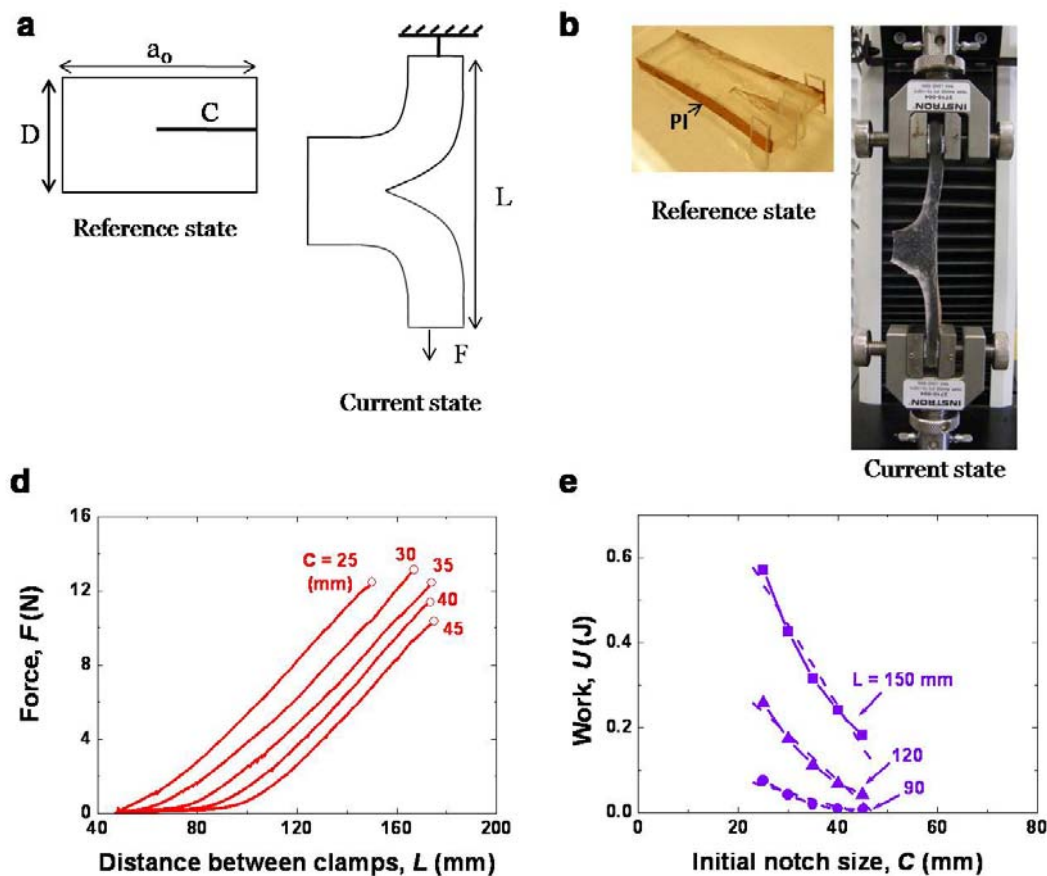

Supplementary Figure 13 | **Verification of the pure shear test method for extremely stretchy materials with tensile test with various crack lengths. a**, Force-extension curves for various crack lengths (C) are plotted, the circles in each curve corresponds to the onset of crack propagation. **b**, The work done in deforming a test piece with various crack lengths was obtained from the area under the force-extension curve with the selected h values.

Double peeling test

In order to verify the pure-shear test for extremely stretchy materials, we also used the double peeling test introduced by Rivlin and Thomas [S10]. Samples with dimensions D = 15mm, a_o = 80mm and thickness b_o = 3mm were prepared with various crack lengths, C as shown in the schematic view in Supplementary Fig. 14a. To prevent the elongation of the arm of sample during stretching, 200 μm thick polyimide films were glued on both side of sample as shown in Supplementary Fig. 14b. Force-extension curves are obtained until the onset of crack propagation for various crack lengths as indicated Supplementary Fig. 14c. The total energy U stored in the test piece at deformation L is obtained by measuring the area under the force-extension curve and U is plotted with the crack lengths C as shown in Supplementary Fig. 14d. A suitable L is selected as 150mm and $\left(\frac{\partial U}{\partial C}\right)_L$ is calculated from the slope of the total energy vs crack length curve. Fracture energy obtained from this method is $7981 \pm 803 \frac{J}{m^2}$ which is comparable with the value of 7350 J/m² obtained from the Rivlin-Thomas pure shear test.


Supplementary Figure 14 | Verification of the pure shear test method for extremely stretchy materials with double peeling test method. a, Schematic figures of the reference state with dimensions D=15mm, a_o=80mm, b_o=3mm and current state after deformation are shown. **b**, Experimental figures of the double peeling test are shown. PI (Polyimide) strips are attached to the two ends of the specimen to control the deformation in the arms. **c**, Force-extension curves for various crack lengths (C) are plotted. **d**, The work done in

deforming a test piece with various crack lengths were obtained from the area under the load-extension curve with selected h values.
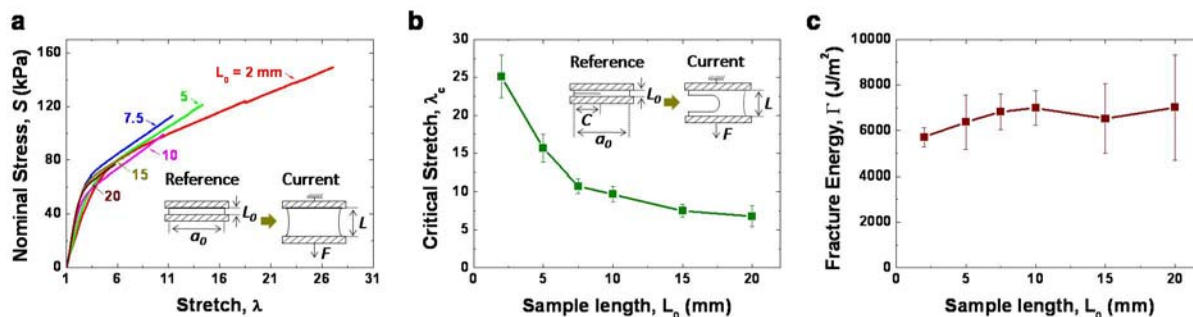
Crack length effect

The effect of the initial crack length was investigated with various crack lengths. We prepared and tested samples of initial crack size C/a_o = 0-0.93. The initial sample length L_o = 5 mm, width a_o = 75 mm, and thickness b_o = 3 mm were fixed for these tests. Alginate-polyacrylamide hybrid gels with 1:8 polymer ratio, 0.0006 MBAA concentration, 0.1328 $CaSO_4$ concentration, and 86.4 wt.% water concentration were used for these tests. Stress- stretch curves were measured with a various crack length until the crack propagation occurred as shown in Supplementary Fig. 15a. The onset crack propagation critical stretches were collected with various crack lengths and plotted in Supplementary Fig. 15b. The critical stretches do not vary much by initial crack lengths in the range of $C/a_o<0.8$. However, the critical stretch decreased to less than half of its value when the ligament length reaches less than 10% of the whole sample width. Fracture energy is calculated and plotted in Supplementary Fig. 15c as a function of crack lengths. As a result, we obtained a consistent fracture energy within the range of $C/a_o<0.8$.
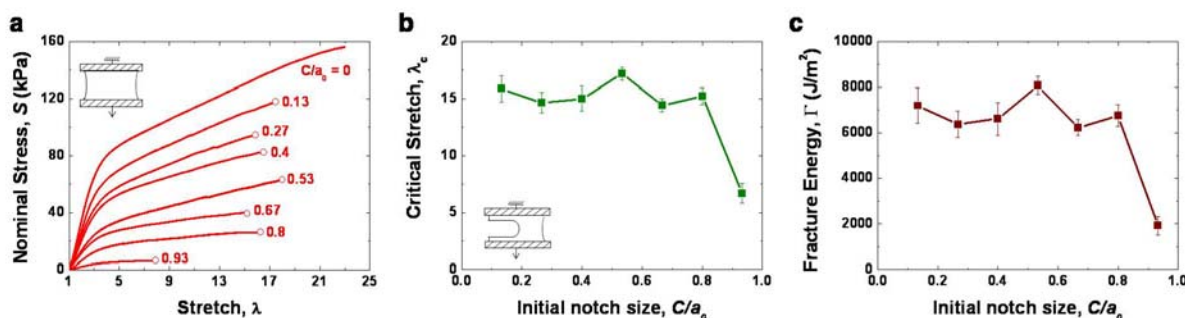
Supplementary Figure 15 | Effect of initial crack length on toughness value. a, Stress- stretch curves for various initial crack lengths, the circles denote the onset of crack propagation. **b**, Critical stretch of the sample with various crack lengths normalized to sample width. **c**, Fracture toughness of the sample as a function of pre-crack length. (Error bars, S.D.; n=3).

Sample size effect

To ascertain that the fracture energy is independent of sample size, we prepared and tested samples of initial lengths L_o = 2-20 mm (Supplementary Fig. 12). The smallest sample, L_o = 2 mm was limited by our experimental setup. The initial sample width a_o = 75 mm, thickness b_o = 3 mm, and notch size $C \approx 0.5a_o$ were fixed for these tests. While the critical stretch decreased with the sample size, the fracture energy remained nearly a constant. Even though the entire sample underwent inelastic deformation, the method yielded a valid test for fracture energy. The situation is similar to testing very ductile metals under large-scale yielding conditions [41]. This experiment indicates that the intrinsic length scale associated with fracture energy is below the minimum sample size used here, L_o = 2 mm. Alginate-polyacrylamide hybrid gels with 1:8 polymer ratio, 0.0006 MBAA concentration, 0.1328 $CaSO_4$ concentration, and 86.4 wt.% water concentration were used for these tests.

Supplementary Figure 16 | Effect of sample length on toughness value. a, Stress-stretch curves for various crack lengths, the circles denote the onset of crack propagation. **b**, Critical stretch of the sample with various sample lengths normalized with sample width. **c**, Fracture toughness of the sample as a function of sample length. (Error bars, S.D.; n=3).

References

31. Annable T., Buscall B., Ettelaie R., and Whittlestone D. The rheology of solutions of associating polymers: comparison of experimental behavior with transient network theory. *J. Rheology* **37**, 695-726 (1993).

32. Kong H. J., Kim C. J., Huebsch N., Weitz D., and Mooney D. J. Noninvasive probing of the spatial organization of polymer chains in hydrogels using fluorescence resonance energy transfer (FRET). *J. Am. Chem. Soc.* **129**, 4518-4519 (2007).

33. Bilodeau G. G. Regular pyramid punch problem. *J. Applied Mech.* **59**, 519-523 (1992).

34. Liang C. X., Hirabayashi K. Improvements of the physical-properties of fibroin membranes with sodium alginate. *J. App. Poly. Sci.* **45**, 1937-1943 (1992).

35. Burrows H. D., Ellis H. A. and Utah S. I. Adsorbed metal ions as stabilizers for the thermal degradation of polyacrylamide. *Polymer* **22**, 1740-1744 (1981).

36. Silva D. A., Paula R. C. M., Feitosa J. P. A. Graft copolymerization of acrylamide onto cashew gum. *European Polymer Journal* **43**, 2620-2629 (2007).

37. Raymond M.-P., Bui V. T. Epoxy/Castor Oil Graft Interpenetrating Polymer Networks. *J. App. Poly. Sci.* **70**, 1649-1659 (1998).

38. Athawale V. D., Lele V. Thermal studies on granular maize starch and its graft copolymers with vinyl monomers. *Starch* **52**, 205-213 (2000)

39. Xue T. J., Wilkie C. A. Thermal degradation of poly(styrene-g-acrylonitrile). *Polymer degradation and stability* **56**, 109-113 (1997).

40. Rivlin, R. S. & Thomas, A. G. Rupture of rubber. I. Characteristic energy for tearing. *J. Polym. Sci.* **10**, 291-318 (1953).

41. Begley, J.A. & Landes, J.D. The J integral as a fracture criterion. *Fracture Toughness, Proceedings of the 1971 National Symposium on Fracture Mechanics, Part II, ASTM STP 514,* American Society for Testing and Materials, pp. 1-20 (1972).

Supplementary Movie 1

This movie shows a crack initiating at the front of a blunted notch, and running rapidly across the sample. A notch was cut into a sample of the hybrid gel. When the gel was stretched, the notch blunted dramatically and remained stable. At a critical applied stretch, a crack initiated at the front of the notch, and ran rapidly through the entire sample. In the undeformed state, the front of the notch was much smaller than the length of the notch. In the deformed state, just before the initiation of the crack, the front was stretched so much that different locations along the front were clearly visible. In this work, however, no effort was made to identify the exact location where the crack was initiated. The alginate-to-acrylamide ratio was 1:8. The covalent crosslinker, MBAA, was fixed at 0.0006 the weight of acrylamide. The ionic crosslinker, $CaSO_4$, was fixed at 0.1993 the weight of alginate. The tests were performed in air, at room temperature, using a tensile machine (Instron model 3342) with a 500-N load cell. The rate of stretch was kept constant at 2 per minute. The real-time movie was recorded at a typical rate of 30 frames/sec.

Supplementary Movie 2

This movie demonstrates large, recoverable deformation when a metal ball drops on a membrane of the hybrid gel. The membrane, thickness 1 mm, was glued to two clamps of polyacrylate with a circular opening, inner diameter 7 cm. A stainless steel ball, diameter 2.54 cm and mass 64 g, was dropped from a high of 1.86 m. Upon hitting the membrane, the ball stretched the membrane greatly, and then bounced back. The membrane remained intact, vibrated, and recovered its initial flat configuration after the vibration was damped out. The alginate-to-acrylamide ratio was 1:4. The covalent crosslinker, MBAA, was fixed at 0.0006 the weight of acrylamide. The ionic crosslinker, $CaSO_4$, was fixed at 0.1328 the weight of alginate. High-speed camera (Vision Research Phantom V711) recorded movies at a typical rate of 6000 frames per second, and a typical exposure time of 160 μs.

Supplementary Movie 3

This movie shows large deformation and rupture when a metal ball drops on a membrane of the hybrid gel. The experimental setup was the same as that in Supplementary Movie 2, except for the size of the steel ball and thickness of gel membrane. A steel ball, diameter 5.08 cm and mass 524 g, was dropped from a high of 1.86 m, and the membrane of the gel used was 2 mm thick. Upon hitting the membrane, the ball stretched the membrane greatly, and caused the membrane to rupture.